Sensors & Actuators: A. Physical 365 (2024) 114920

Contents lists available at ScienceDirect

Sensors and Actuators: A. Physical

journal homepage: www.journals.elsevier.com/sensors-and-actuators-a-physical

Self-sensing characteristics of smart high-performance cementitious composites containing multiwall carbon nanotubes, steel fibers, and steel slag aggregates under compression

Huy Viet Le [a,b,*], Van Manh Nguyen [a,b], Thi Nhan Pham [a,b], Van Lam Tang [a,b], Xuan Nui Pham [c], Duy Liem Nguyen [d], Dong Joo Kim [e]

[a] Department of Building and Construction Engineering, Faculty of Civil Engineering, Hanoi University of Mining and Geology, Hanoi, Vietnam
[b] Geotechnical Engineering, Construction Materials and Sustainability Research Group, Hanoi University of Mining and Geology, Hanoi, Vietnam
[c] Department of Chemical Engineering, Hanoi University of Mining and Geology, Hanoi, Vietnam
[d] Faculty of Civil Engineering, Ho Chi Minh City University of Technology and Education, Ho Chi Minh City, Vietnam
[e] Department of Civil Engineering and Environment, Sejong University, Seoul, South Korea

ARTICLE INFO

Keywords:
Smart high-performance cementitious composite
MWCNT
Self-sensing
Steel fiber
Steel slag aggregate

ABSTRACT

Smart high-performance cementitious composite (SHPCC) with sensing abilities, high mechanical, and high durability is a potential smart material instead of current sensors applied for structural health monitoring systems of infrastructures. This study deeply investigated the sensing properties of SHPCCs containing multiwall carbon nanotubes (MWCNTs), steel fibers, and steel slag aggregates (SSAs) under compression. SHPCCs containing different contents of MWCNTs (0.1% and 0.5% of cement weight), steel fibers (2 and 4 vol%), SSAs (10% and 50% instead of sand), and free water (fully dried and moisture specimens) were prepared and evaluated. The results indicated that the SSA content was a key factor controlling the electrically conductive network response and the stress-sensing ability of SHPCCs. MWCNTs significantly enhanced the stress-sensing ability of fully dried SHPCCs under compression. Besides, the free water content in pore systems significantly influenced the stress-sensing ability of SHPCCs. A conductive network of SHPCCs with MWCNTs, fibers, SSAs, and free water at micro and nano levels was proposed and analyzed to explain the electrical resistivity response under compression.

1. Introduction

The collapse of infrastructures and buildings without warning caused a huge economic loss and numerous human deaths. Some catastrophic collapses of structures have recently occurred such as Dhaka Savar Rana Plaza in Bangladesh, in 2013 (1134 deaths), the Sampoong department store in Korea, in 1995 (502 human deaths), Morandi Bridge in Italy, in 2018 (43 deaths), and Brumadinho dam in Brazil, 2019 (270 deaths). Structural health monitoring (SHM) systems of structures have become an interesting topic for researchers and engineers to prevent sudden collapses. However, current sensors (strain gauge, lead zirconate titanate (PZT), and fiber Bragg grating (FBG) sensors) in SHM systems had drawbacks such as a high cost, low durability in comparison with the structural life cycle, a localized application, and influencing mechanical properties of structures with embedded sensors. Smart high-performance cementitious composites (SHPCCs) with self-sensing abilities and high mechanical properties have been recently developed to overcome the drawbacks of current sensors to apply to SHM systems.

A potential application of SHPCCs was to fabricate a smart anchorage block (SAB) [1–3] which was used as an anchorage head of prestressed concrete structures. The SAB can monitor the change in stress and ruptures of prestressed tendons, which are the main reasons causing the catastrophic collapse of infrastructures [1–3]. SHPCCs with high compressive strength and durability can resist high compressive stress

Abbreviations: AC, alternative current; CCP, continuous conductive path; CP, conductive path; DCP, discontinuous conductive path; DP, discontinuous point; FCR, the fractional change in electrical resistivity; FD, fully dried; FF, functional filler; FWC, free water content; ICP, insulator conductive path; MWCNT, multiwall carbon nanotube; SHPCC, smart high-performance cementitious composite; SSA, steel slag aggregate; SSC, stress sensitive coefficient.

* Corresponding author at: Department of Building and Construction Engineering, Faculty of Civil Engineering, Hanoi University of Mining and Geology, Hanoi, Vietnam.
E-mail address: lehuyviet@humg.edu.vn (H.V. Le).

https://doi.org/10.1016/j.sna.2023.114920
Received 9 September 2023; Received in revised form 28 November 2023; Accepted 7 December 2023
Available online 15 December 2023

caused by prestressed tendons at the anchorage head (approximately 50 MPa) [3] and work as a high-stress sensor to monitor the stress loss or the collapse of tendons. The sensing ability of SHPCCs was observed by evaluating the fractional change in electrical resistivity (FCR) under external loading [4]. As tendons of prestressed structures were ruptured, based on a significant change in the FCR of the SAB owing to a notable change in the compressive stress, the SHM system can immediately detect and send a warning about abnormal structures in real time for central management. Hence, infrastructures would be repaired, reinforced, or maintained to avoid sudden catastrophic collapses.

High electrically conductive functional fillers (FFs) such as carbon fibers, carbon blacks, carbon nanotubes (CNTs), multi-wall carbon nanotubes (MWCNTs), graphene, carbon black, steel fibers, steel slag aggregates (SSAs), or hybrid FFs were generally added into cementitious composites to improve the conductive network and the FCR of cementitious composites [4–27]. However, the stress sensing of these studies has been limited to under 20 MPa which is notably lower than the stress sensing requirement of SAB (around 50 MPa) because of the low strength of cementitious composites.

The dispersion of FFs in SHPCCs was more difficult than that in conventional cementitious composites because SHPCCs had a lower water-per-cement ratio and a denser microstructure. You et al. [28] reported that MWCNTs improved the electrical conductivity of SHPCCs but decreased the flow (even more than 50% superplasticizer was added) and the compressive strength because of insufficient dispersion of MWCNTs. Recently, Lee et al. [29] reported that SSAs and steel fibers would be easily dispersed and work as FFs in SHPCCs. They reported that a hybrid of SSAs and steel fibers produced a better self-sensing ability of SHPCCs than a single FF. Le et al. [9] investigated the effects of SSA size and content investigated the effects of different SSA sizes (0.39 mm, 1–2 mm, and 3–4 mm in maximum diameter) and contents (0.3, 0.5, 1.0, 1.5, and 2.0 in SSAs per cement ratio) incorporating 1 and 2 vol% steel fibers on the stress sensing ability of SHPCCs. They indicated that a finer SSA size (0.39 mm in maximum diameter) produced a better dispersion and consequently higher FCR than coater SSA sizes. In addition, SHPCCs containing 2 vol% steel fibers and 50% SSAs instead of sand provided the highest FCR under compression. Le et al. [30] indicated that the FCR of SHPCCs clearly increased as the fiber content increased from 2 to 4 vol% but little changed as the fiber content increased from 4 to 5 vol%. In addition, a combination of 4 vol% steel fibers and 50% SSA instead of sand produced the highest FCR at the elastic region (30% maximum compressive stress). Le et al. [31] reported that the electrical resistivity of SHPCCs was significantly dependent upon the free water content (FWC) inside the composite. Nevertheless, the sensing ability of SHPCCs without FWC (i.e. fully dried specimens) was not observed owing to significant data noises in the electrical resistivity under compression [31]. Le et al. [32] reported that adding 0.1% MWCNTs by cement weight ratio, 2 vol% steel fibers, and 50% SSAs (instead of sand) improved the FCR of SHPCCs in comparison with SHPCCs containing a hybrid of steel fibers and SSAs or copper slag or nickel aggregates. They observed that a combination of nano FF (MWCNTs), particle FF (SSAs), and fibers (steel fibers) would maximize the sensing ability of SHPCCs. However, these studies have not indicated which parameter mainly controlled the sensing characteristic of SHPCCs containing MWCNTs, SSAs, and steel fibers. Moreover, the effects of MWCNT content on the sensing properties of SHPCCs have not been investigated. In addition, the effect of FWC on the self-sensing of SHPCCs under compression has not been investigated. This study aims to deeply investigate the self-sensing ability of SHPCCs containing MWCNTs, steel fibers, and SSAs under high compressive stress and solve the limitations of current studies.

2. Electrical resistivity characteristics of smart concretes

The electrically conductive network in the smart cementitious composites included ionic, contacting, and tunneling conductions [4]. The ionic conduction was based on the movement of ions (K+, Na+, OH−) in porous systems, which were significantly affected by the composite microstructure [4]. The contacting conduction depended on the content and the type of FFs [4,32,33]. The tunneling conduction of closed enough FFs (under 10 nm) was influenced by the content, shape, and electrical conductivity of FFs [4,9,29,34,35].

Under compression, as the compressive strain increased, the tunneling and contacting conduction increased because the distance between FFs decreased and the number of FF contact increased. However, Han et al. [4] indicated that as the FF content was over the percolation threshold, well-stable conductive pathways were generated into the composites, and thus the conductive network or the electrical resistivity of the composites little changed under external loads. Hence, depending on FF types, the FF content should be controlled under a percolation threshold.

Alternative current (AC) or direct current (DC) measurements were generally used to obtain the electrical resistance of smart cementitious composites [10,12,29,36]. The AC measurement method was preferably utilized to prevent the effects of polarization and contacting resistance between electrodes and matrix [32,36,37]. The electrical resistivity (ρ) of self-sensing specimens was calculated from a measured electrical resistance (R_c) according to Eq. (1) [29,37].

$$\rho = R_c \frac{A}{L}, \tag{1}$$

where A is the cross-sectional area and L is the gauge length between two electrodes.

To evaluate the electrical property under external loads, the FCR was generally determined and evaluated. The FCR was determined following Eq. (2) [4].

$$\mathrm{FCR} = |(r - r_o)|/r_o.100\%, \tag{2}$$

where ρ_o is the initial electrical resistivity and ρ is the electrical resistivity at the calculated point). Besides, the stress-sensitive coefficient (SSC) was calculated following Eq. (3) [4,32].

$$\mathrm{SSC} = \mathrm{FCR}/s, \tag{3}$$

where σ is the compressive stress at the calculated point.

3. Experiments

An experimental program was designated to evaluate the mechanical and sensing properties of SHPCCs containing MWCNTs, steel fibers, and SSAs under high compressive stress. The contents of MWCNTs, steel fibers, and SSAs were chosen based on gaps in current studies [9,29–32] to find which parameter mainly controlled the sensing characteristics of SHPCCs under compression. Besides, the content of MWCNTs generally varied from 0.1 to 1% by weight of cement [19,26,38–40]. However, as the nano FF content increased, their dispersion into SHPCCs would be more difficult. Thus, in this study, SSAs content instead of sand, steel fiber content, the MWCNT content by cement weight varied from 10% to 50%, 2 to 4%, and 0.1 to 0.5%, correspondingly to deeply understand the effects of FF types including fiber, particle, and nano FFs on the sensing properties of SHPCCs. Furthermore, the effects of adding MWCNTs on the self-sensing ability of SHPCCs with/without free water (F2S10_FD, F2C01S10_FD, and F2C01S10 with FWC, where FD means fully dried specimens) were investigated. Table 1 summarizes the compositions of SHPCC matrices by weight ratio.

3.1. Materials

Cement Type I (ASTM standard) and silica fume (10 μm in diameter) were utilized as binders in the matrix composition. Silica powder and silica sand have average diameters of 74 μm (200# mesh) and 0.2 mm, respectively. A low water-per-cement ratio of 0.2 and a superplasticizer-

Table 1
Compositions of SHPCC matrices by weight ratio.

No.	Cement	Silica fume	Silica powder	Silica sand	SSA	Water	SP	Fiber (vol%)	*MWCNT*	
F2C01	1.0	0.15	0.25	1.0	-	0.2	0.108	2.0	0.001	
F2C05	1.0	0.15	0.25	1.0	-	0.2	0.108	2.0	0.005S	
F2C01S10	1.0	0.15	0.25	0.9	0.1	0.2	0.108	2.0	0.001	
F4C01S10	1.0	0.15	0.25	0.9	0.1	0.2	0.108	2.0	0.001	
F2C01S50	1.0	0.15	0.25	0.9	0.1	0.2	0.096	2.0	0.001	[32]
F2S10_FD	1.0	0.15	0.25	0.9	0.1	0.2	0.108	2.0	-	
F2C01S10_FD	1.0	0.15	0.25	0.9	0.1	0.2	0.108	2.0	0.001	

SP: superplasticizer with 30% solid and 70% water. FD: fully dried SHPCCs with no free water.

based polycarboxylate were used to generate high compressive strength and workability for SHPCCs. Short smooth straight steel fibers with 6 mm in length, 0.2 mm in diameter, 360 GPa in elastic modulus, and 2104 MPa in tensile strength were added to enhance the crack resistance, the tensile strength, and the sensing ability of SHPCCs. MWCNTs with 5–10 nm in diameter, 10 μm in length, 150–200 m^2/g in specific surface area analysis (BET), higher 99% in purity, and 0.02–0.04 g/cm^3 in bulk density provided by Carbon Nano-material Technology Co., LTD [41] were utilized to reinforce the conductive network of SHPCCs at the nano level.

SSAs with a sphere shape and a maximum diameter of 0.39 mm were instead of a part of sand in SHPCC compositions and worked as an FF to improve the conductive network as well as the self-sensing ability of SHPCCs. SSAs are produced by Ecomaister Company using slag atomizing technology [42] and are significantly different from conventional SSAs using other technologies. The chemical properties of SSAs include 13.10% SiO_2, 6.31% Al_2O_3, 24.1% CaO, 3.68% MgO, 38.3% Fe_2O_3, and 14.01% others. Wang et al. [43] reported that free-CaO was a primary component that caused the soundness of SSAs. As the content of free-CaO is 4.96%, the SSA has bad soundness while as it is 2.09%, the SSA shows satisfactory soundness over 4 years [43]. Ecomaister Company reported that SSA has below 0.15% free-CaO and volume stability [42]. In addition, SSAs have a spinel structure (an octahedron-shaped structure) and a complex oxide formed at the spinel structure surface, which resulted in the difficult ion or electron movement in chemical reactions and generating a stable compound as well as very strong physical and chemical resistances [42]. Even so, the effect of SSA volume stability on structural safety in the long term should be further considered. Fig. 1 shows the images of electrically conductive FFs including MWCNTs (Fig. 1a), steel fibers (Fig. 1b), and SSAs (Fig. 1c).

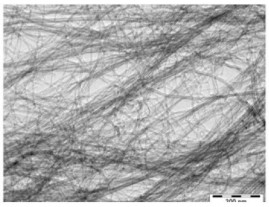

a) MWCNT_MR99 [41]

b) Steel fibers (6 mm in length)

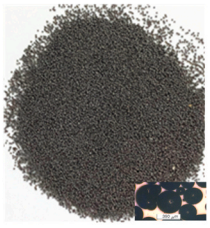

c) SSAs (0.39 mm in maximum diameter)

Fig. 1. Functional filler images.

3.2. Specimen preparation

Fig. 2 presents processes to prepare SHPCCs containing MWCNTS using the SSS method. Besides, an SS method was conducted in comparison with the SSS method. The details of the SS method and test results regarding the SS method were presented in the supporting files. Based on the tested results in the supporting file, the SSS dispersion method, which provided better workability and compressive strength, was utilized to disperse MWCNTs into SHPCC matrices. The SSS method contained steps as follows: (1) MWCNTs, water, and a half of superplasticizer were stirred for 1 min; (2) a sonication with an amplitude of 50% was applied to a solution of MWCNTs, water, and superplasticizer for 120 min [32,40,44]; (3) cement, silica sand, SSAs, and silica powder were dried mixed for 5 min, and then they were taken out the mixer; (4) the above solution was mixed with the silica fume in the mixer for 3 min; then (5) the dried mixed materials in step 3 were added into the mixture and further mixed for 3 min; (6) superplasticizer was slowly added and the mixture was continuously mixed for 3 min; (7) flow test was conducted; and (8) the mixture was finally poured into compressive molds with size of $50\times50\times50$ mm^3 and applied a slight vibration to reduce air bubbles in matrices.

To prepare SHPCCs containing steel fibers, short steel fibers were manually added, and the mixture was further mixed for 3 min. Then, the fresh mixtures were poured into compressive molds. At least three specimens of each matrix were prepared to determine the compressive strength of matrices. Two-wire meshes (45 mm and 70 mm in width and height, respectively) were embedded in the self-sensing specimens as electrodes with a distance of 20 mm to observe electrical properties under compression. All specimens were covered by a plastic sheet and kept in the laboratory room at a temperature of 20 ± 2 °C for 48 h. After demolding, specimens were stored in a hot water tank (controlled temperature of 90 °C) for 72 h. Then, they were continuously kept in the laboratory room for 24 h before testing.

To evaluate the effect of the addition of MWCNTs on the self-sensing ability of fully dried SHPCCs, fully dried specimens without FWC were prepared. Specimens were cured in an oven with a controlled temperature of 80 °C for approximately 3 days (until the weight of specimens was stable). The FWC in the SHPCC specimens was determined following Eq. (4).

$$FWC = \left(W - W_{fd}\right)/W_{fd.}100\%, \quad (4)$$

where W is the weight of initial specimens and W_{fd} is the weight of fully dried specimens [31].

3.3. Test setup

Fig. 3 shows the test setup for observing the compressive stress and electrical properties of SHPCC specimens. A universal testing machine (UTM, 300 tf capacity) with a load speed of 1.0 mm/minute was utilized to apply the compressive load. The compressive stress was obtained by a load cell attached to the UTM machine. An SI 1260 impedance/gain-phase analyzer (an alternative current (AC) machine) with a fixed frequency of 100 Hz based on [29] was used to measure the electrical resistance between two probes of self-sensing specimens. Plastic sheets

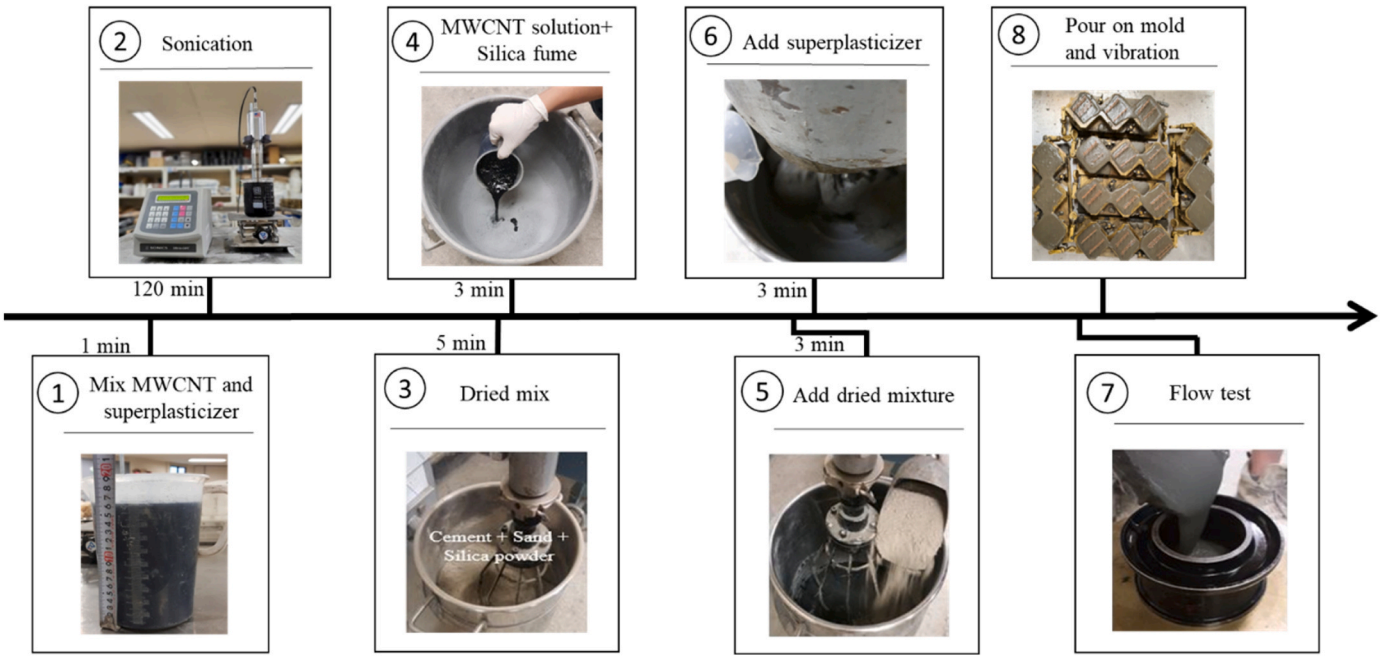

Fig. 2. Process to disperse MWCNT into SHPCC matrices using an SSS method.

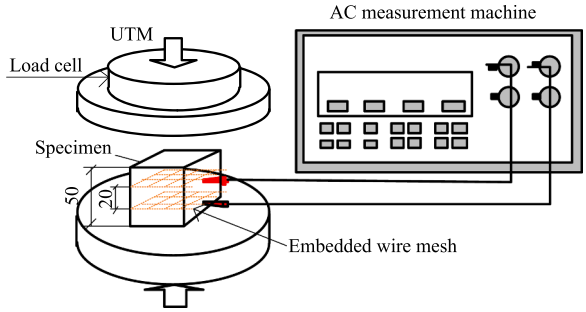

Fig. 3. Test set-up for measuring electrical resistance of specimens under compression.

were put on the contact surfaces of self-sensing specimens with the UTM to avoid the contacting UTM effect on the electrical resistance measurement (R_c). At least three specimens were tested for each SHPCC matrix.

A Hitachi SU8010 machine with scanning electron microscope (SEM) and EDX functions was utilized to analyze the microstructure of HPCCs. SEM specimens were prepared according to the steps in [37]. A back-scattered electron signal with 15 kV voltage at a low-vacuum condition was set to capture SEM images. EDX was utilized to analyze the chemical components and the MWCNT distribution through C element distribution for the SEM specimen of SHPCC matrices.

4. Test results and discussions

Fig. 4 shows the electrical resistivity response of SHPCCs under compression. Continuous lines illustrate the ratio of the determined electrical resistivity and the initial electrical resistivity (ρ_x and ρ_o, respectively) while discontinuous lines present compressive stress. Fig. 4a and b show responses of SHPCCs with different contents of MWCNT. Fig. 4c–f show the effects of MWCNTs incorporating different contents of fiber, SSA, and free water on the electrical resistivity response of SHPCCs. Table 2 summarizes the maximum compressive stress, ρ_o at the initial testing point, $\Delta\rho = \rho_p - \rho_o$, FCR, σ_m, and the stress-sensitive coefficient (SSC = FCR/σ_p) at the maximum compressive stress point of SHPCCs.

4.1. Mechanical characteristics of SHPCCs

Fig. 5 compares the maximum compressive stress value of SHPCCs. The maximum compressive stress of SHPCC matrices slightly decreased from 138.0 MPa (F2C01) to 134.2 MPa (F2C05) as the MWCNT content increased from 0.1% to 0.5% by cement weight, as summarized in Table 2. Isfahani et al. [40] also reported a reduction in the compressive strength of cementitious composites with increasing the MWCNT content. You et al. [45] observed a significant reduction in the compressive strength of SHPCCs as the MWCNT content increased from 0.1% to 0.5%. A higher MWCNT content (0.5%) would produce more weak zones (MWCNT agglomerates), which caused a lower compressive strength of F2C05.

The maximum compressive stress of F2C01S10 (130.1 MPa) was slightly lower than that of F2C01S50 (138.6 MPa [32]). Le et al. [32] also obtained an increase in the compressive strength of SHPCC as the content of SSA instead of sand increased from 10% to 50%. As the SSA content increased, the flowability of the SHPCC matrix increased [9,29,32]. Air bubbles in a higher flowability matrix would be easier to exit from the fresh matrix owing to vibration and resulted in a denser microstructure of the matrix and a higher maximum compressive stress [46].

The compressive strength of the SHPCC matrix notably increased from 130.1 to 157.8 MPa as the fiber content increased from 2 vol% (F2C01S10) to 4 vol% (F4C01S10). Le et al. [30] also indicated that as the fiber volume content increased from 2 to 5 vol%, the compressive strength significantly increased because of the effects of fibers bridging micro-cracks. A higher number of fibers bridging micro-cracks or pores into SHPCC matrices improved the micro-crack resistance and consequently increased the matrix compressive strength.

Fig. 6 illustrates the microstructure of SHPCC with MWCNTs (F2C01S10) using the SSS dispersion method. EDX analysis results of the composite were summarized in Table S3 in the supporting file. As shown in Fig. 6, the microstructure of the matrix surrounding SSAs was highly dense and contained discontinuous microcracks (Fig. 6a and b). Besides, the FWC of the SHPCC matrix determined according to Eq. (4) was around 1.8%. Le et al. [31] obtained that the FWC of SHPCCs with

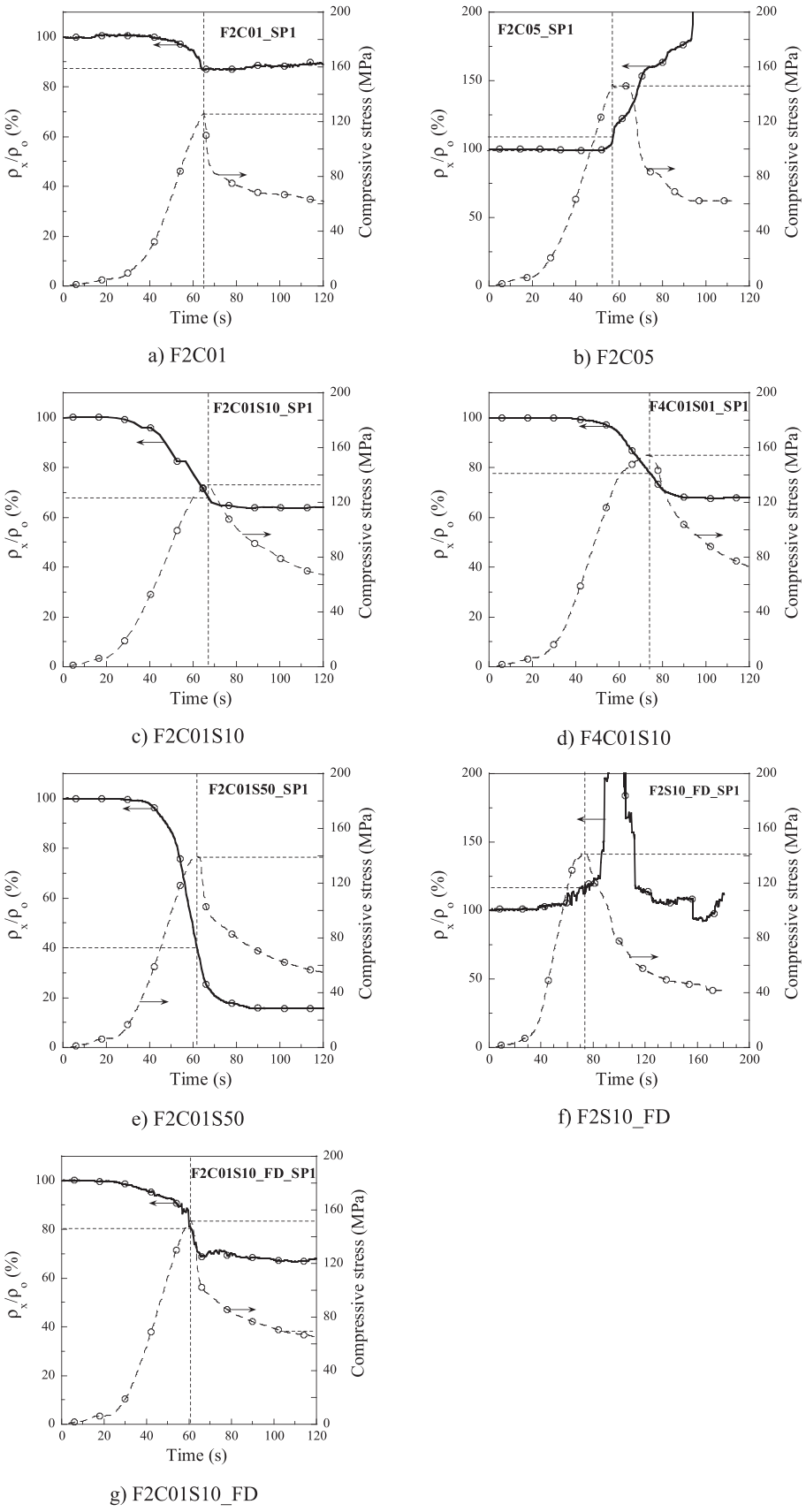

Fig. 4. Electrical resistivity responses of SHPCCs under compression.

Table 2
Self-stress sensing characteristics of SHPCCs.

Notation	Maximum stress, σ_p, (MPa)	Initial resistivity, ρ_o (kΩ-cm)	$\Delta\rho = \rho_o - \rho_p$ (kΩ-cm)	FCR_p (%)	SSC (%/MPa)	Note
F2C01	138.0 (10.5)	595.1 (23.9)	82.9	13.9 (3.4)	0.101	
F2C05	134.2 (11.9)	126.3 (3.0)	-12.3	9.7 (3.8)	0.072	
F2C01S10	130.1 (2.9)	434.7 (37.8)	115.3	26.2 (4.4)	0.201	
F2C01S50	138.6 (8.1)	189.1 (9.4)	107.3	56.8 (1.4)	0.410	[32]
F4C01S10	157.8 (4.0)	86.77 (41.5)	13.4	15.4 (2.2)	0.098	
F2S10_FD	144.3 (4.8)	5230.6 (850.2)	Noise	Noise	-	
F2C01S10_FD	143.5 (10.4)	1846.4 (142.6)	272.1	14.6 (3.0)	0.102	

The standard deviation was typed in brackets. FD: fully dried specimens.

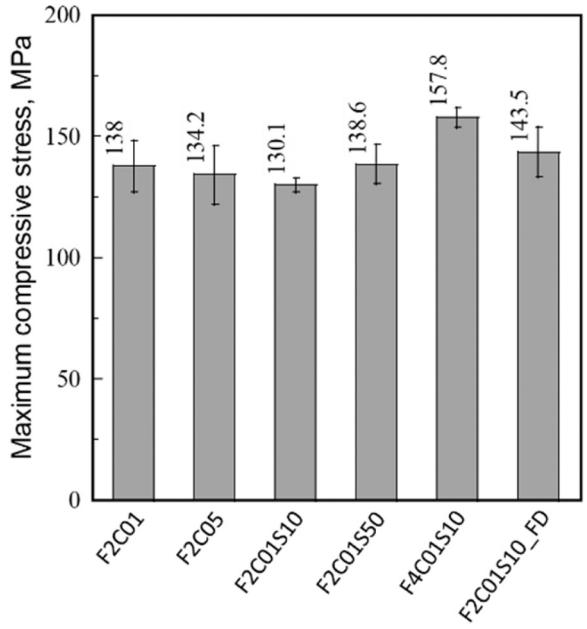

Fig. 5. The maximum compressive stress of SHPCCs.

178–184 MPa in the compressive strength varied from 1.2% to 1.4% while Le et al. [47] reported that the porosity of conventional cementitious composites (61.9–76.4 MPa in the compressive strength) was changed from 11% to 15%. Nochaiya et al. [48] reported that EDX results can be utilized to confirm and determine the quantity of MWCNT dispersion in cementitious composites. As shown in Fig. 6c, the C element was well dispersed into the matrix. Besides, a high amount of C in the ITZ (12.49% by weight ratio (wt%) in Table S3) indicated that the high amount of MWCNTs was dispersed into the SHPCC matrix. Nochaiya et al. [48] reported a good dispersion of MWCNTs in the cementitious composites as the C element in the cementitious matrix was 10.23 wt%. Furthermore, the amount of Si, Ca, O, and Al were 12.90, 11.07, 54.81, and 1.61 wt%, respectively, which presented the composition of hydration products.

4.2. *Self-sensing properties of SHPCCs under compression*

4.2.1. *Electrical resistivity responses of SHPCCs under compression*

The electrical resistivity response of SHPCCs (Fig. 4a, c, d, e, and g) can be divided into three main stages as follows: (1) the electrical resistivity of SHPCCs increases with increasing compressive stress until peak stress; (2) the electrical resistivity of SHPCCs continuously decreased to a minimum electrical resistivity after peak stress; and (3) the electrical resistivity of SHPCCs was little changed or gradually increased. [9,30,32] also reported three stages in the electrical resistivity response of SHPCCs containing short smooth steel fibers and other FFs under compression.

Fig. 4b shows a different trend in the electrical resistivity response with two stages of F2C05 containing 0.5% MWCNTs. In stage 1, the electrical resistivity of composites was little changed until peak stress. In stage 2, it notably increased after the compressive stress started to decrease. In stage 1, a high-volume content of FFs (0.5% MWCNTs and 2 vol% steel fibers) would generate a well conductive network in the matrix and consequently produce a stable response under compression. In stage 2, after peak stress, as the compressive strain continuously increased, opening cracks would destroy the conductive network and cause an increase in the electrical resistivity of composites.

The addition of MWCNTs significantly improved the electrical resistivity response of fully dried SHPCC specimens under compression. As can be seen in Fig. 4f, F2S10_FD specimens with no FWC produced a significant data noise in the electrical resistivity whereas F2C01S10_FD specimens without FWC (Fig. 8g) did not provide the data noise in the electrical resistivity under compression. Le et al. [31] also obtained the data noise in the electrical resistivity of fully dried SHPCCs containing 2 vol% steel fibers and 50% SSA instead of sand under compression. The FWC and MWCNTs in SHPCC specimens mainly influenced the data noise in the electrical resistivity response. Le et al. [31] reported that the electrical resistivity of fully dried specimens was equal to around two times that of moisture specimens containing 1.2–1.4% FWC [31]. As summarized in Table 2, the electrical resistivity of F2C01S01_FD (1846.4 kΩ-cm) was notably higher than that of F2C01S01 (434.7 kΩ-cm of moisture specimens). Under high compression, as the compressive strain increased, the contacting and tunneling conductions of FFs increased. Whereas the propagation and opening of micro-cracks caused an increase in the electrical resistivity of composites, which would result in the electrical resistivity data noise of fully dried specimens. The FWC would provide the ionic conduction in porous or micro-crack systems while MWCNTs bridging micro-cracks would produce tunneling and contacting conductions of MWCNTs. Thus, SHPCCs with FWC or MWCNTs did not observe data noise in the electrical resistivity.

4.2.2. *The stress sensing characteristics of SHPCCs*

Fig. 7 compares the FCR and the SSC of SHPCCs containing MWCNTs, steel fibers, and SSAs. A combination of MWCNTs, short steel fibers, and SSAs in F2C01S50 produced the highest FCR and SSC for SHPCCs under compression. As summarized in Table 2, F2C01S50 produced the highest FCR up to 56.8%. SSAs mainly controlled the FCR of SHPCCs containing nano FF, microparticle FF, and macro fiber FF under high compression.

A controlled content of SSAs was easier to maximize the distance between FFs and the FCR of SHPCCs than controlled contents of MWCNTs and steel fiber. As the SSA content increased from 10% to 50%, the FCR notably increased from 26.2% of F2C01S10 to 56.8% of F2C01S50 (116% increase). Le et al. [32] also obtained that as the SSA content increased from 10% to 50%, the FCR of SHPCCs containing SSAs and 2 vol% steel fibers significantly increased from 26.5 to 42.9%. However, as the SSA content increased from 50 to 100%, the FCR of SHPCCs containing SSAs and steel fibers decreased to 34.4% [9].

Table 3 listed the number of fibers (N_f), the number of fiber contacts

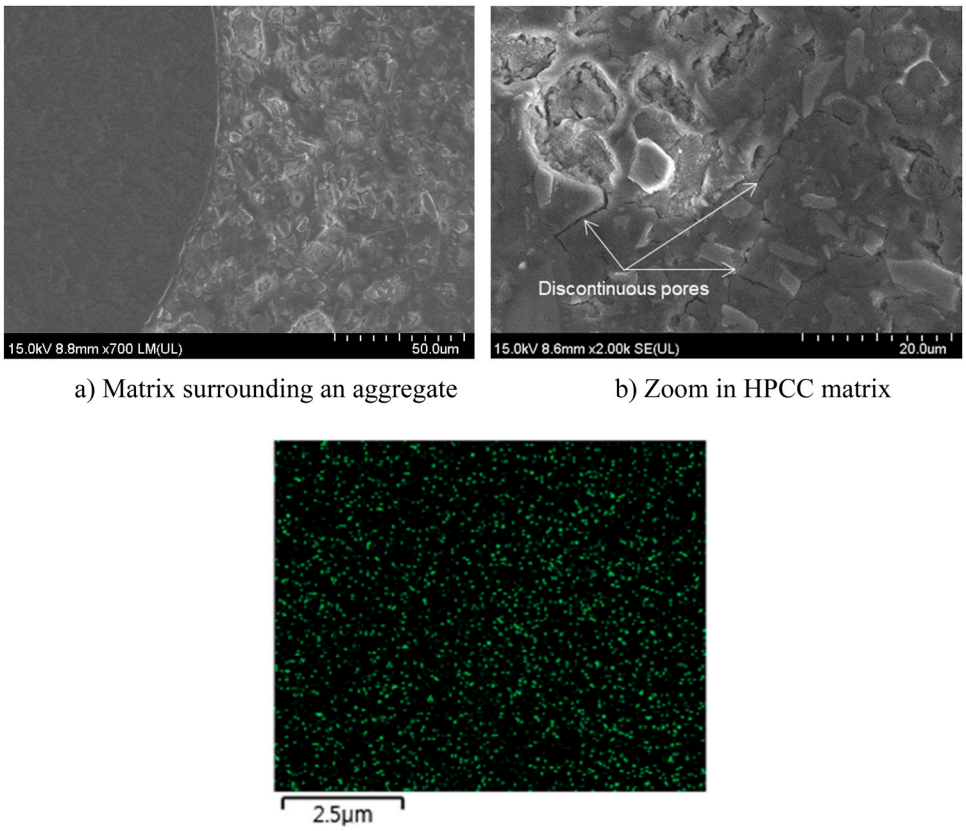

a) Matrix surrounding an aggregate b) Zoom in HPCC matrix

c) EDX image of C element distribution in the SHCC matrix

Fig. 6. SEM images of SHPCC matrix with MWCNT.

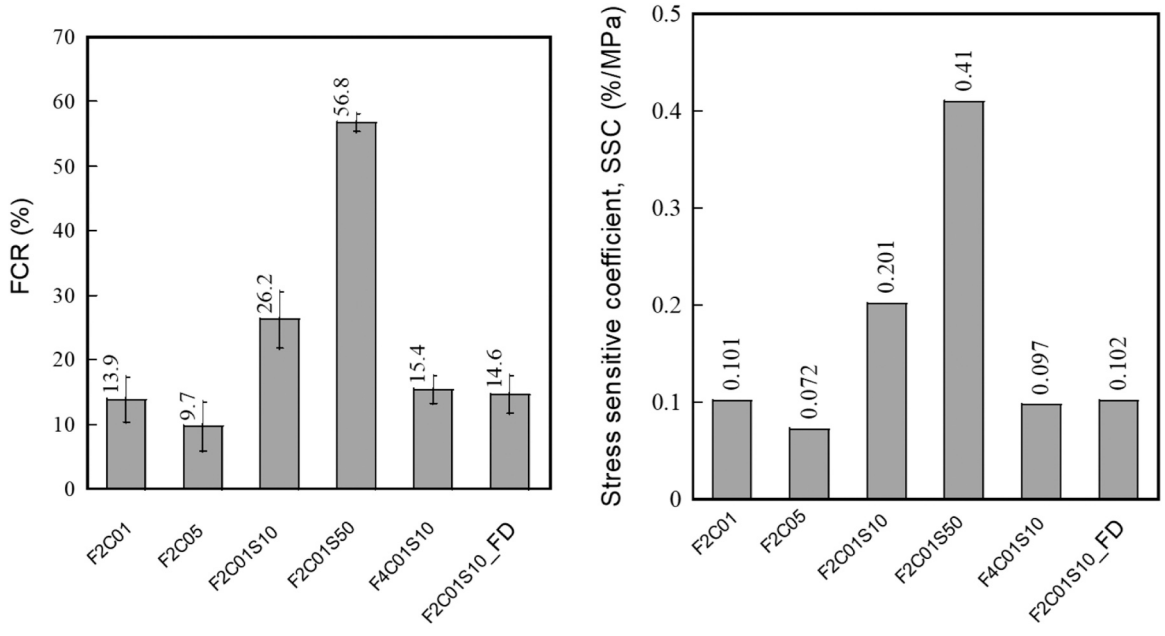

a) FCR b) SSC

Fig. 7. FCR and SSC of SHPCCs.

Table 3
N_f, N_c, N_p, N_n, and L of SHPCCs.

Test series	N_f	Nc	N_p	L (μm)	Nn	Note
F2C01	13,262	10,465	-	-	5390,386,9365,908	
F2C05	13,262	10,465	-	-	269,519,346,829,539	
F2S10_FD	13,262	10,465	103,378	675.4	-	
F2C01S10	13,262	10,465	103,378	675.4	53,903,869,365,908	
F2C01S50	13,262	10465	550,396	220.1	53,903,869,365,908	[32]
F4C01S10	26,525	22,606	103,378	675.4	53,903,869,365,908	

(N_c), the number of SSA particles (N_p), the distance between SSA particles (L), and the number of MWCNTs (N_n). N_f and N_n were determined according to Eq. (5) while N_c was calculated according to Eq. (6) [32]. Assuming that SSAs were uniformly distributed in the composites, N_p and L were determined by using Eq. (7) and Eq. (8) [32], respectively.

$$N_f = \frac{V_o \cdot V_c}{V_F} = \frac{V_o \cdot V_c}{\pi d_f^2 \Big] \Big/ 4} \tag{5}$$

$$N_c = \frac{8 V_C \cdot V_o \cos^{-1}\left(\frac{13.8 d_j}{l}\sqrt{\frac{1}{V_c}}\right)}{\left(\pi d_j\right)^2 l} \tag{6}$$

$$N_p = \frac{V_S . V_C}{V_{sp}} = \frac{V_S . V_C}{\frac{4}{3}\pi . \left(\frac{d_x}{2}\right)^3} \tag{7}$$

$$L - d_x \cdot \left(\left(\frac{\pi}{6}\right)^{1/3}\right) \cdot V_S^{(-1/3)} - 1 \tag{8}$$

where V_F and V_C are volumes of a fiber and the composite, respectively; d_f, l, and V_o are the diameter, length, and volume fraction of electrically conductive fibers, respectively. V_S and V_{sp} are the volume of an SSA and the volume content of SSAs in the matrix, respectively; d_s is the SSA diameter.

As summarized in Table 3, the distance between SSAs was 220 μm and 675.4 μm in matrices of F2C01S50 and F2C01S10, respectively while the diameter of fibers was 200 μm and sizes of MWCNTs were 10 nm and 10 μm in diameter and length. Hoang et al. [49] reported that under compression, the strain of high performance cementitious composites (around 150 MPa in compressive strength) containing steel fibers at the peak stress was from 0.417 to 0.449%. Assuming that, the strain of SHPCCs in this study was 0.410% at peak stress, the size of the SHPCCs in the 20 mm gauge length measurement would decrease 82 μm. Thus, at peak stress, the F2C01S50 containing 50% SSAs, 2 vol% steel fibers, and 0.1% MWCNTs by cement weight would produce a closed enough distance and connections between FFs (MWCNTs, SSAs, and steel fibers) and result in a higher FCR than other SHPCCs. In the F2C01S01 matrix, the distance between SSAs was 674.4 μm, which was notably higher than the total fiber diameter and MWCNT length and could not maximize the FCR of SHPCCs at peak stress. In contrast, as the SSA content was 100% instead of sand, the distance between SSAs was 66.5 μm [9], which clearly lowered the fiber diameter (200 μm) and consequently produced over percolation threshold of the conductive pathways in the SHPCC matrix and a lower FCR.

Furthermore, as the MWCNT content increased from 0.1% to 0.5%, the FCR decreased from 13.9% of F2C01 to 9.7% of F2C05. The electrical resistivity of F2C05 was little changed before peak stress and significantly increased after peak stress (Fig. 4b). The content of FFs including steel fibers and MWCNTs in F2C05 would be over the percolation threshold, which generates a little change in electrical resistivity before peak stress under compression [4,29,32]. However, F2C05 illustrated a potential application for the damage sensing of SHPCCs after peak stress. You et al. [28] also reported a significant increase in the electrical resistivity of SHPCC with MWCNTs (0.5% by weight cement ratio) and steel fibers under compression after matrix cracking. The generation and propagation of micro-cracks at the micro level after peak stress would destroy the contacting and tunneling conductions between nanomaterials (MWCNTs) at the nano level in the conductive network and consequently increase the electrical resistivity of SHPCCs with increasing compressive strain.

Besides, as the fiber content increased from 2 vol% to 4 vol%, the FCR decreased from 26.2% of F2C01S10 to 15.4% of F4C01S10 (41% decrease). Le et al. [30] reported that as the steel fiber content increased from 2 to 4 vol%, the FCR of SHPCCs significantly increased from 20.5% to 33.5%. However, the FCR of SHPCCs containing 5 vol% was 33.7% [30]. Thus, 4 vol% fiber content in SHPCCs would be near to a percolation threshold. A combination of 4 vol% steel fiber, SSAs, and MWCNTs in F4C01S10 would be slightly higher than the percolation threshold and generate a well-initially conductive pathway in composites. Thus, as the compressive strain increased, the change in the conductive network of FFs in F4C01S10 was less than that in F2C01S10.

Hence, a controlled content of SSAs was easier to improve the FCR of SHPCCs than fibers and MWCNTs. In addition, the distance between SSAs should be controlled to a slightly higher total fiber diameter and MWCNT length.

The FWC significantly influenced the FCR of SHPCCs under compression. As shown in Fig. 7, FCR values of F2C01S10 with FWC and F2S01C01_FD without FWC were 26.2% and 14.6%, respectively. Even nano FFs (MWCNTs) can help to improve the electrical resistivity response and reduce the data noise by connecting FFs at nano or micro levels, the connection of FWC and FFs in SHPCCs would significantly influence the FCR under external loads. A significant decrease (44%) in the FCR of F2C01S10_FD indicated that the FWC had an important role in influencing the self-sensing ability of SHPCCs.

4.2.3. A conductive network model of SHPCCs

Fig. 8 illustrates a conductive network of MWCNTs, FFs, and FWC at the micro (Fig. 8a) and the nano (Fig. 8b) levels, a simplified conductive network in SHPCCs (Fig. 8c), and a circuit model for SS-HPCCs (Fig. 8d). Le et al. [32] also proposed a conductive model for SHPCCs containing MWCNTs, steel fibers, and SSAs. However, the FWC had not been considered and the conductive pathway in the model also had not been analyzed in detail. Besides, Song et. al. [50] first proposed a simplified conductive network for concretes without FFs. At the micro level, the continuous conductive path (CCP) in SHPCC matrices would include (1) conductive paths of FFs such as fibers with fibers, fibers with SSAs or MWCNTs, and a combination of fiber, SSAs, and MWCNTs; and (2) conductive paths between FFs and pore system. The movement of ions in pores/crack solution systems generated ionic conduction [4]. As mentioned above part, the microstructure of SHPCC matrices was highly dense and contained discontinuous pores and cracks. Wang et al. [51] indicated that the microstructure of cementitious composites with a higher 150 MPa in compressive strength contained no continuous pore system. Thus, a continuous conductive path of only ionic conduction in pore solution systems in the gauge length of two electrodes would be difficult to generate. Gel particles (hydration and pozzolanic reaction products), un-hydration binders (cement and silica fume), aggregates (silica sand or silica powder), and pores/cracks without FWC produced

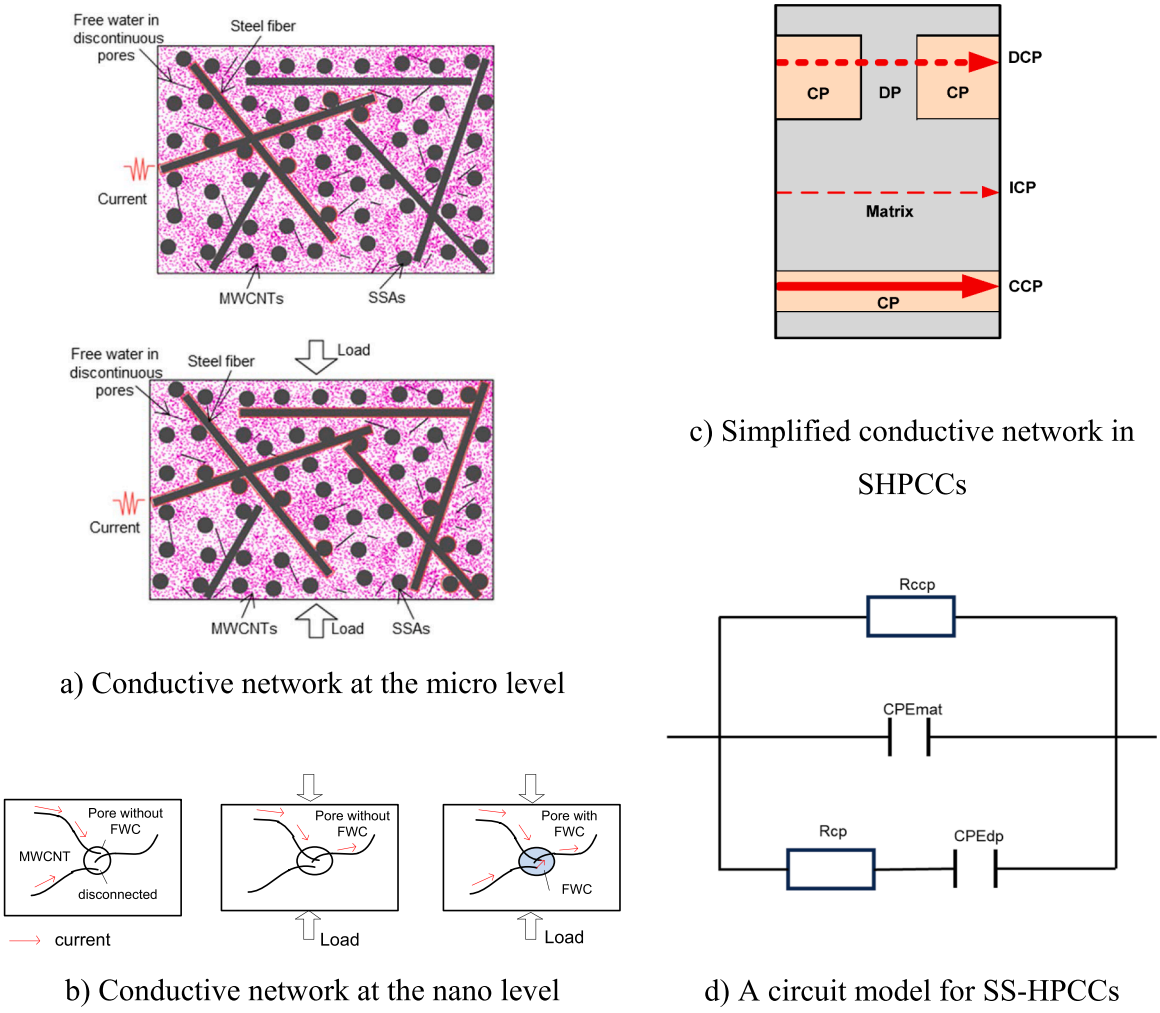

Fig. 8. Conductive network and circuit models of SHPCCs containing a mixture of different FFs under compression.

the discontinuous point (DP) or insulators in the conductive network. In dried specimens, pores/cracks became DPs or insulators. At the nano level, the presence of free water filled pores or cracks and the contact of nano FFs (MWCNTs) enhanced the conductive pathway between FFs (Fig. 8b) and consequently improved the sensing property of SHPCCs under external loads.

As the compressive stress/strain increased, the connection of FFs (fibers, SSAs, and MWCNTs) or FFs and pore systems at both micro and nano levels generated a more conductive pathway and resulted in changing DCPs to CCPs. Whereas as cracks were generated and opened in matrices, they would destroy CCPs in matrices and consequently change CCPs back to DCPs. In stage 1, as the compressive stress/strain increased, the distance between FFs decreased, the number of FF connections (fibers, SSAs, and MWCNTs) increased, and consequently contacting and tunneling conductions of FFs increased. Besides, the ionic conduction was enhanced because the movement of ions was enhanced with increasing the compressive stress [52]. Thus, the electrical resistivity decreased owing to increasing the additional CCPs changed from DCPs. In stage 2, as the compressive strain continuously increased, the compressive stress decreased while main cracks were generated, propagated, and opened. [9,13,18,53,54] reported that the connection of steel fibers bridging cracks with a high electrical conductivity caused a decrease in the electrical resistivity of composites. Fiber bridging cracks mainly controlled the electrical resistivity response of SHPCCs after matrix cracking [12]. Thus, even after the peak stress, the number of additional CCPs was still greater than additional DCPs. The electrical resistivity of composites reached a minimum value as the conductive network of FFs and FWC had been already stable unless increasing the compressive strain. In stage 3, as the number of cracks and the crack width significantly increased, the pull-out of fibers and opening cracks in matrices produced a slight increase in the electrical resistivity of composites as the CCPs changed to the DCPs.

Fig. 8d shows a proposed circuit model of a conductive pathway through three parallel parts in the SS-HPCCs based on the proposed conductive network in Fig. 8c. Li and Li [50] also proposed a circuit model including three parallel paths like that in Fig. 8d for an un-cracked path of cementitious composites containing carbon blacks. R_{ccp} presents the electrical resistance of a continuous conductive path (CCPs) in the electrical current direction. CPE_{mat} illustrates the electrical capacitance of matrices between conductive pathways. CPE_{dp} and R_{CP} connected in series represent the electrical capacitance between partially conductive paths and the electrical resistance of partially conductive paths, respectively.

5. Conclusions

This study deeply investigated the sensing properties of SHPCCs containing MWCNTs, steel slag aggregates, and steel fibers under compression. The conclusions could be drawn as follows:

- The microparticle FF (SSAs) mainly controlled the FCR of SHPCCs containing nano FF, microparticle FF, and macro fiber FF under high compression. A controlled content of SSAs was easier to maximize the distance between FFs and the FCR of SHPCCs than controlled

contents of MWCNTs and steel fiber. In addition, the distance between SSAs should be controlled to a slightly higher total fiber diameter and MWCNT length.

- The addition of MWCNTs significantly improved the electrical resistivity response of fully dried SHPCC specimens under compression. MWCNTs significantly decreased the electrical resistivity data noise of SHPCCs containing no free water under compression.
- The free water content significantly influenced the electrical resistivity response and the FCR of SHPCCs containing MWCNTs, SSAs, and steel fibers. The FCR of fully dried specimens (F2C01S10_FD) decreased by 44% compared to that of moisture specimens (F2C01S10).
- A conductive network at micro and nano levels was proposed and analyzed to explain the sensing characteristics of SHPCCs under compression.

Author statement

Dr. Huy Viet Le has conducted experiments and prepared initial draft versions of the manuscript and the rebuttal. Dr. Van Manh Nguyen, Dr. Thi Nhan Pham, Dr. Van Lam Tang, Dr. Xuan Nui Pham, and Dr. Duy Liem Nguyen reviewed and revised the initial draft versions. And, Dr. Dong Joo KIM designed the experimental program and revised the initial draft versions.

CRediT authorship contribution statement

Nguyen Van Manh: Writing – review & editing. **Pham Thi Nhan:** Writing – review & editing. **Tang Van Lam:** Writing – review & editing. **Pham Xuan Nui:** Writing – review & editing. **Le Viet Huy:** Conceptualization, Investigation, Supervision, Writing – original draft. **Nguyen Duy Liem:** Writing – review & editing. **Kim Dong Joo:** Conceptualization, Writing – review & editing.

Declaration of Competing Interest

The authors declare the following financial interests/personal relationships which may be considered as potential competing interests: Huy Viet Le reports financial support was provided by Education and Training Ministry Vietnam.

Data availability

Data will be made available on request.

Acknowledgments

This research was supported by the Basic Research Program funded by the Education and Training Ministry (Project B2022-MDA-05). The opinions expressed in this paper are those of the authors and do not necessarily reflect the views of the sponsors.

Appendix A. Supporting information

Supplementary data associated with this article can be found in the online version at doi:10.1016/j.sna.2023.114920.

References

[1] T.U. Kim, M.K. Kim, J.W. Park, D.J. Kim, Effects of temperature and humidity on self-stress sensing capacity of smart concrete blocks, J. Build. Eng. 69 (2023), 106227, https://doi.org/10.1016/j.jobe.2023.106227.
[2] D.J. Kim, H.W. Noh, S.I. Choi, R.H. Hwang, S.Y. Lee, Smart concrete anchoragefor monitoring pre-stressing loss, 2019.
[3] S.Y. Lee, H.V. Le, M.K. Kim, D.J. Kim, J. Park, An innovative smart concrete anchorage with self-stress sensing capacity of prestressing stress of PS tendon, Sensors 21 (2021), https://doi.org/10.3390/s21155251.
[4] B. Han, X. Yu, J. Ou, Self-sensing concrete in smart structures, Butterworth Heinemann, Elsevier, Kidlington, 2014, https://doi.org/10.1016/C2013-0-14456-X.
[5] S. Wen, D.D.L. Chung, Piezoresistivity in continuous carbon fiber cement-matrix composite, Cem. Concr. Res. 29 (1999) 445–449, https://doi.org/10.1016/S0008-8846(98)00211-7.
[6] X. Fu, W. Lu, D.D.L. Chung, Improving the strain-sensing ability of carbon fiber-reinforced cement by ozone treatment of the fibers, Cem. Concr. Res. 28 (1998) 183–187, https://doi.org/10.1016/S0008-8846(97)00265-2.
[7] X. Wang, S. Wang, D.D.L. Chung, Sensing damage in carbon fiber and its polymer-matrix and carbon-matrix composites by electrical resistance measurement, J. Mater. Sci. 34 (1999) 2703–2713.
[8] D.D.L. Chung, Self-monitoring structural materials, Mater. Sci. Eng. R. Rep. 22 (1998) 57–78, https://doi.org/10.1016/S0927-796X(97)00021-1.
[9] H.V. Le, D.H. Lee, D.J. Kim, Effects of steel slag aggregate size and content on piezoresistive responses of smart ultra-high-performance fiber-reinforced concretes, Sens. Actuators A Phys. 305 (2020), 111925, https://doi.org/10.1016/j.sna.2020.111925.
[10] H.V. Le, D.J. Kim, Effect of matrix cracking on electrical resistivity of high performance fiber reinforced cementitious composites in tension, Constr. Build. Mater. 156 (2017) 750–760, https://doi.org/10.1016/j.conbuildmat.2017.09.046.
[11] H.V. Le, T.U. Kim, S. Khan, J.Y. Park, J.W. Park, S.E. Kim, J. Yun, D.J. Kim, Development of low-cost wireless sensing system for smart ultra-high performance concrete, Sensors 21 (2021) 1–20, https://doi.org/10.3390/s21196386.
[12] D.L. Nguyen, J. Song, C. Manathamsombat, D.J. Kim, Comparative electromechanical damage-sensing behaviors of six strain-hardening steel fiber-reinforced cementitious composites under direct tension, Compos. Part B Eng. 69 (2014) 159–168, https://doi.org/10.1016/j.compositesb.2014.09.037.
[13] J. Song, D.L. Nguyen, Effect of fiber volume content on electromechanical behavior of cementitious composites, (2015). https://doi.org/10.1177/0021998314568169.
[14] D.Y. Yoo, S. Kim, S.H. Lee, Self-sensing capability of ultra-high-performance concrete containing steel fibers and carbon nanotubes under tension, Sens. Actuators A Phys. 276 (2018) 125–136, https://doi.org/10.1016/j.sna.2018.04.009.
[15] B. Han, J. Ou, Embedded piezoresistive cement-based stress/strain sensor, Sens. Actuators A Phys. 138 (2007) 294–298, https://doi.org/10.1016/j.sna.2007.05.011.
[16] S. Ding, Y. Ruan, X. Yu, B. Han, Y. Ni, Self-monitoring of smart concrete column incorporating CNT/NCB composite fillers modified cementitious sensors, Constr. Build. Mater. 201 (2019) 127–137, https://doi.org/10.1016/j.conbuildmat.2018.12.203.
[17] S.J. Lee, D. Ahn, I. You, D.Y. Yoo, Y.S. Kang, Wireless cement-based sensor for self-monitoring of railway concrete infrastructures, Autom. Constr. 119 (2020), 103323, https://doi.org/10.1016/j.autcon.2020.103323.
[18] H.V. Le, D.J. Kim, Effects of matrix strength, fiber type, and fiber content on the electrical resistivity of steel-fiber-reinforced cement composites during fiber pullout, J. Korean Soc. Civ. Eng. 39 (2019) 675–689.
[19] M.S. Konsta-Gdoutos, P.A. Danoglidis, M.G. Falara, S.F. Nitodas, Fresh and mechanical properties, and strain sensing of nanomodified cement mortars: The effects of MWCNT aspect ratio, density and functionalization, Cem. Concr. Compos. 82 (2017) 137–151, https://doi.org/10.1016/j.cemconcomp.2017.05.004.
[20] M.S. Konsta-gdoutos, A.A. Chrysoula, Self sensing carbon nanotube (CNT) and nanofiber (CNF) cementitious composites for real time damage assessment in smart structures, Cem. Concr. Compos. 53 (2014) 162–169, https://doi.org/10.1016/j.cemconcomp.2014.07.003.
[21] P.A. Danoglidis, M.S. Konsta-Gdoutos, E.E. Gdoutos, S.P. Shah, Strength, energy absorption capability and self-sensing properties of multifunctional carbon nanotube reinforced mortars, Constr. Build. Mater. 120 (2016) 265–274, https://doi.org/10.1016/j.conbuildmat.2016.05.049.
[22] Y. Wang, S. Sun, L. Zhang, Self-sensing cementitious composites incorporating hybrid NGPs/CNTs/NCBs for structural health monitoring, Sens. Actuators A Phys. 357 (2023), 114365, https://doi.org/10.1016/j.sna.2023.114365.
[23] Y. Wang, L. Zhang, Development of self-sensing cementitious composite incorporating hybrid graphene nanoplates and carbon nanotubes for structural health monitoring, Sens. Actuators A Phys. 336 (2022), 113367, https://doi.org/10.1016/j.sna.2022.113367.
[24] S. Ding, Y. Xiang, Y.Q. Ni, V.K. Thakur, X. Wang, B. Han, J. Ou, In-situ synthesizing carbon nanotubes on cement to develop self-sensing cementitious composites for smart high-speed rail infrastructures, Nano Today 43 (2022), 101438, https://doi.org/10.1016/j.nantod.2022.101438.
[25] S. Ding, X. Wang, L. Qiu, Y.Q. Ni, X. Dong, Y. Cui, A. Ashour, B. Han, J. Ou, Self-sensing cementitious composites with hierarchical carbon fiber-carbon nanotube composite fillers for crack development monitoring of a maglev girder, Small 19 (2023), https://doi.org/10.1002/smll.202206258.
[26] B. Han, Z. Yang, X. Shi, X. Yu, Transport properties of carbon-nanotube/cement composites, J. Mater. Eng. Perform. 22 (2013) 184–189, https://doi.org/10.1007/s11665-012-0228-x.
[27] B. Han, K. Zhang, X. Yu, E. Kwon, J. Ou, Electrical characteristics and pressure-sensitive response measurements of carboxyl MWNT/cement composites, Cem. Concr. Compos. 34 (2012) 794–800, https://doi.org/10.1016/j.cemconcomp.2012.02.012.
[28] I. You, D.Y. Yoo, S. Kim, M.J. Kim, G. Zi, Electrical and self-sensing properties of ultra-high-performance fiber-reinforced concrete with carbon nanotubes, Sensors 17 (2017) 1–19, https://doi.org/10.3390/s17112481.

[29] S.Y. Lee, H.V. Le, D.J. Kim, Self-stress sensing smart concrete containing fine steel slag aggregates and steel fibers under high compressive stress, Constr. Build. Mater. 220 (2019) 149–160, https://doi.org/10.1016/j.conbuildmat.2019.05.197.
[30] L.H. Viet, L. Dao Phuc, N.T. Thuong, N.T. Thanh, D.L. Nguyen, D.J. Kim, Improvement of the stress sensing ability of ultra-high-performance concrete using short steel fibers and steel slag aggregates under high compression, Sens. Actuators A. Phys. 362 (2023), 114616, https://doi.org/10.1016/j.sna.2023.114616.
[31] H.V. Le, M.K. Kim, D.J. Kim, J. Park, Electrical properties of smart ultra-high performance concrete under various temperatures, humidities, and age of concrete, Cem. Concr. Compos. 118 (2021), 103979, https://doi.org/10.1016/j.cemconcomp.2021.103979.
[32] H.V. Le, M.K. Kim, S.U. Kim, S.-Y. Chung, D.J. Kim, Enhancing self-stress sensing ability of smart ultra-high performance concretes under compression by using nano functional fillers, J. Build. Eng. 44 (2021), 102717, https://doi.org/10.1016/j.jobe.2021.102717.
[33] S. Wen, D.D.L. Chung, A comparative study of steel- and carbon-fibre cement as piezoresistive strain sensors, Adv. Cem. Res. 15 (2003) 119–128, https://doi.org/10.1680/adcr.15.3.119.36621.
[34] H. Xiao, H. Li, J. Ou, Modeling of piezoresistivity of carbon black filled cement-based composites under multi-axial strain, Sens. Actuators A. Phys. 160 (2010) 87–93, https://doi.org/10.1016/j.sna.2010.04.027.
[35] J. Xu, W. Zhong, W. Yao, Modeling of conductivity in carbon fiber-reinforced cement-based composite, J. Mater. Sci. (2010) 3538–3546, https://doi.org/10.1007/s10853-010-4396-5.
[36] B. Han, S. Ding, X. Yu, Intrinsic self-sensing concrete and structures: a review, Measurement 59 (2015) 110–128, https://doi.org/10.1016/j.measurement.2014.09.048.
[37] M.K. Kim, H.V. Le, D.J. Kim, Electromechanical response of smart ultra-high performance concrete under external loads corresponding to different electrical measurements, Sens. (Switz.) 21 (2021) 1–19, https://doi.org/10.3390/s21041281.
[38] S. Sasmal, N. Ravivarman, B.S. Sindu, K. Vignesh, Electrical conductivity and piezo-resistive characteristics of CNT and CNF incorporated cementitious nanocomposites under static and dynamic loading, Compos. Part A Appl. Sci. Manuf. 100 (2017) 227–243, https://doi.org/10.1016/j.compositesa.2017.05.018.
[39] H.K. Kim, I.S. Park, H.K. Lee, Improved piezoresistive sensitivity and stability of CNT/cement mortar composites with low water-binder ratio, Compos. Struct. 116 (2014) 713–719, https://doi.org/10.1016/j.compstruct.2014.06.007.
[40] F. Torabian Isfahani, W. Li, E. Redaelli, Dispersion of multi-walled carbon nanotubes and its effects on the properties of cement composites, Cem. Concr. Compos. 74 (2016) 154–163, https://doi.org/10.1016/j.cemconcomp.2016.09.007.
[41] ⟨www.carbonnano.co.kr⟩, (n.d.).
[42] ⟨www.ecomaister.com⟩, (n.d.).
[43] Q. Wang, D. Wang, S. Zhuang, The soundness of steel slag with different free CaO and MgO contents, Constr. Build. Mater. 151 (2017) 138–146, https://doi.org/10.1016/j.conbuildmat.2017.06.077.
[44] B. Han, X. Yu, E. Kwon, J. Ou, Effects of CNT concentration level and water / cement ratio on the piezoresistivity of CNT / cement composites, J. Compos. Mater. 46 (I) (2011) 19–25, https://doi.org/10.1177/0021998311401114.
[45] I. You, D.Y. Yoo, S. Kim, M.J. Kim, G. Zi, Electrical and self-sensing properties of ultra-high-performance fiber-reinforced concrete with carbon nanotubes, Sensors 17 (2017), https://doi.org/10.3390/s17112481.
[46] J. Yang, B. Chen, J. Su, G. Xu, D. Zhang, J. Zhou, Effects of fibers on the mechanical properties of UHPC: a review (English Ed., in: J. Traffic Transp. Eng, 9, 2022, pp. 363–387, https://doi.org/10.1016/j.jtte.2022.05.001 (English Ed.
[47] H.V. Le, D. Moon, D.J. Kim, Effects of ageing and storage conditions on the interfacial bond strength of steel fibers in mortars, Constr. Build. Mater. 170 (2018) 129–141, https://doi.org/10.1016/j.conbuildmat.2018.03.064.
[48] T. Nochaiya, P. Tolkidtikul, P. Singjai, A. Chaipanich, Microstructure and characterizations of portland-carbon nanotubes pastes, Adv. Mater. Res. 55–57 (2008) 549–552, https://doi.org/10.4028/www.scientific.net/amr.55-57.549.
[49] A. Le Hoang, E. Fehling, Influence of steel fiber content and aspect ratio on the uniaxial tensile and compressive behavior of ultra high performance concrete, Constr. Build. Mater. 153 (2017) 790–806, https://doi.org/10.1016/j.conbuildmat.2017.07.130.
[50] G. Song, Equivalent circuit model for AC electrochemical impedance spectroscopy of concrete, Cem. Concr. Res. 30 (2000) 1723–1730, https://doi.org/10.1016/S0008-8846(00)00400-2.
[51] D. Wang, C. Shi, Z. Wu, J. Xiao, Z. Huang, Z. Fang, A review on ultra high performance concrete: part II. Hydration, microstructure and properties, Constr. Build. Mater. 96 (2015) 368–377, https://doi.org/10.1016/j.conbuildmat.2015.08.095.
[52] M. Sun, Z. Li, X. Song, Piezoelectric effect of hardened cement paste, Cem. Concr. Compos. 26 (2004) 717–720, https://doi.org/10.1016/S0958-9465(03)00104-5.
[53] D.L. Nguyen, D.J. Kim, D.K. Thai, Enhancing damage-sensing capacity of strain-hardening macro-steel fiber-reinforced concrete by adding low amount of discrete carbons, Materials 16 (2019), https://doi.org/10.3390/ma12060938.
[54] H.V. Le, D.J. Kim, Detecting crack and damage location in self-sensing fiber reinforced cementitious composites, Constr. Build. Mater. 240 (2020), 117973, https://doi.org/10.1016/j.conbuildmat.2019.117973.

Huy Viet Le, Ph.D., Lecturer: Department of Civil Engineering, Hanoi University of Mining and Geology, Hanoi, Vietnam, 18 Vien street, Bac Tu Liem District, Hanoi, Vietnam.

Van Manh Nguyen, Ph.D., Associate Professor: Department of Civil Engineering, Hanoi University of Mining and Geology, Hanoi, Vietnam, 18 Vien street, Bac Tu Liem District, Hanoi, Vietnam.

Thi Nhan Pham, Ph.D., Lecturer: Department of Civil Engineering, Hanoi University of Mining and Geology, Hanoi, Vietnam, 18 Vien street, Bac Tu Liem District, Hanoi, Vietnam.

Van Lam Tang, Ph.D., Lecturer: Department of Civil Engineering, Hanoi University of Mining and Geology, Hanoi, Vietnam, 18 Vien street, Bac Tu Liem District, Hanoi, Vietnam.

Xuan Nui Pham, Ph.D., Associate Professor: Department of Chemical Engineering, Hanoi University of Mining and Geology, Hanoi, Vietnam, 18 Vien street, Bac Tu Liem District, Hanoi, Vietnam.

Duy Liem Nguyen, Ph.D., Associate Professor: Faculty of Civil Engineering, Ho Chi Minh City University of Technology and Education, 01 Vo Van Ngan, Thu Duc District, Ho Chi Minh City, Vietnam.

Dong Joo Kim, Ph.D., Professor: Department of Civil and Environmental Engineering, Sejong University, 98 Gunja-Dong, Gwangjin-Gu, Seoul 143–747, Republic of Korea.